Thiamin Biosynthesis in *Bacillus subtilis*: Structure of the Thiazole Synthase/Sulfur Carrier Protein Complex[†,‡]

Ethan C. Settembre, Pieter C. Dorrestein, Huili Zhai, Abhishek Chatterjee, Fred W. McLafferty, Tadhg P. Begley,* and Steven E. Ealick*

Department of Chemistry and Chemical Biology, Cornell University, Ithaca, New York 14853

Received May 31, 2004; Revised Manuscript Received July 8, 2004

ABSTRACT: Thiazole synthase is the key enzyme involved in the formation of the thiazole moiety of thiamin pyrophosphate. We have determined the structure of this enzyme in complex with ThiS, the sulfur carrier protein, at 3.15 Å resolution. Thiazole synthase is a tetramer with 222 symmetry. The monomer is a $(\beta\alpha)_8$ barrel with similarities to the aldolase class 1 and flavin mononucleotide dependent oxidoreductase and phosphate binding superfamilies. The sulfur carrier protein (ThiS) is a compact protein with a fold similar to that of ubiquitin. The structure allowed us to model the substrate, deoxy-D-xylulose 5-phosphate (DXP), in the active site. This model identified Glu98 and Asp182 as new active site residues likely to be involved in the catalysis of thiazole formation. The function of these residues was probed by mutagenesis experiments, which confirmed that both residues are essential for thiazole formation and identified Asp182 as the base involved in the deprotonation at C3 of the thiazole synthase DXP imine. Comparison of the ThiS binding surface to the surface of ubiquitin identified a conserved hydrophobic patch of unknown function on ubiquitin that may be involved in complex formation between ubiquitin and one of its binding partners.

Thiamin pyrophosphate is an essential cofactor in all living systems and plays a key role in the stabilization of acyl carbanion intermediates involved in carbohydrate and amino acid metabolism. The cofactor consists of a pyrimidine covalently linked to a thiazole. The thiazole moiety is biosynthesized in *Bacillus subtilis* and in most other bacteria from 1-deoxy-D-xylulose 5-phosphate (**1**, DXP),[1] glycine, and cysteine in a complex oxidative condensation reaction requiring five different proteins. Of these, ThiS is the sulfur carrier protein and carries the sulfur needed for thiazole assembly on its carboxy terminus (ThiS−COSH). ThiG is the thiazole synthase and catalyzes the formation of the thiazole from DXP (**1**), ThiS−COSH (**2**), and dehydroglycine (**3**) (*1*−*3*) (Scheme 1).

Thiazole synthase complexed with the sulfur carrier protein consists of a tetramer of ThiS/thiazole synthase heterodimers. ThiS is a 7.2 kDa protein with a ubiquitin-like fold, and thiazole synthase is a 26.9 kDa protein. The mechanism of the early steps catalyzed by thiazole synthase have been elucidated, and an imine between the DXP substrate and lysine 96 has been characterized (*4*). The thiazole synthase sequence is highly conserved in bacteria and shows similarity to thiamin phosphate synthase, a member of the flavin mononucleotide dependent oxidoreductase and phosphate binding (FMOP) superfamilies of $(\beta\alpha)_8$ barrel enzymes.

Scheme 1

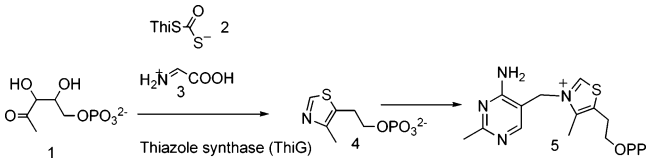

The recently determined solution structure of *Escherichia coli* ThiS provided strong evidence for a potential evolutionary relationship to ubiquitin, ubiquitin-like proteins (ubls), and MoaD, the sulfur carrier protein involved in the biosynthesis of molybdopterin (*5*). ThiS, ubquitin/ubls, and MoaD are each activated through adenylation at a conserved C-terminal Gly-Gly motif by their activating enzymes ThiF, E1, and MoeB, respectively. The high sequence identity among the activator proteins and the similarity of their substrates indicated that they may be functionally analogous (*6*). MoaD complexed with its adenylating protein MoeB (*7*) and NEDD8 complexed with its adenylating protein AP-PBP1-UBA3 (*8*) showed structural similarities and provided structural details of the adenylation mechanism. The current evidence suggests that ubiquitin and other ubls derive from an ancestral sulfur carrying system related to ThiS and MoaD (*9*).

[†] This work was supported by National Institutes of Health Grants DK44083 (to T.P.B.), GM16609 (to F.W.M.), and RR15301 (to S.E.E.). S.E.E. is indebted to the W. M. Keck Foundation and the Lucille P. Markey Charitable Trust.

[‡] The Brookhaven Protein Data Bank code for the thiazole synthase/ThiS complex is 1TYG.

* To whom correspondence should be addressed. Telephone: (607) 255-7961. Fax: (607) 255-1227. E-mail addresses: see3@cornell.edu or tbp2@cornell.edu.

[1] Abbreviations: DXP, deoxy-D-xylulose 5-phosphate; ubls, ubiquitin-like proteins; ALD1, aldolase class 1; FMOP, flavin mononucleotide dependent oxidoreductase and phosphate binding; IPTG, isopropyl-β-D-thiogalactoside; SeMet, selenomethionine; LB, Luria-Bertani media; KP_i, potassium phosphate; PEG 8K, poly(ethylene glycol) 8000; DTT, dithiothreitol; APS, Advanced Photon Source; ESI-FTMS, electron spray ionization-Fourier transform mass spectrometry; FBPA, fructose 1,6-(bis)phosphate aldolase; FBPA 1A, fructose 1,6-(bis)phosphate aldolase class 1A; TtFBPA, *Thermoproteus tenax* fructose 1,6-(bis)-phosphate aldolase.

10.1021/bi0488911 CCC: $27.50
Published on Web 08/21/2004

Here we describe the structure of *B. subtilis* thiazole synthase complexed to the sulfur carrier protein ThiS. The evolutionary implications of the structural similarity of ThiS to ubiquitin are described. We will also propose that the thiazole synthase structure represents the strongest link between the FMOP and ALD1 superfamilies suggesting a common evolutionary precursor. Finally, the implications of an active site model for the mechanism of thiazole biosynthesis will be discussed.

MATERIALS AND METHODS

Protein Copurification. The native proteins were obtained by transforming pCLK820, encoding ThiS (with a 10× N-terminal histidine tag) and thiazole synthase, into the *E. coli* overexpression strain BL21(DE3) (Novagen) (*3*). A 5 mL starter culture of these cells was used to inoculate 1 L of LB containing 50 μg/mL ampicillin. The cells were grown at 37 °C to an OD_{600} of ~0.6 and then induced with 500 μM isopropyl-β-D-thiogalactoside (IPTG). After an additional 6 h, the cells were spun down at 4420 × *g* for 10 min and stored at −80 °C.

For production of the selenomethionine (SeMet) incorporated proteins, the methionine auxotrophic strain of *E. coli*, B834(DE3) (Novagen), was transformed with pCLK820 and grown as described above with the following modifications. The SeMet growth medium contained M9 salts plus 0.4% (w/v) glucose, 2 mM $MgSO_4$, 25 μg/mL $FeSO_4 \cdot 7H_2O$, 1 mM $CaCl_2$, 50 μg/mL ampicillin, and 1% BME vitamin solution (GibcoBRL) supplemented with 40 μg/mL of all amino acids except L-methionine, which was replaced with L-SeMet. Cells from an initial overnight 5 mL starter culture, grown in LB containing 50 μg/mL of ampicillin, were washed with SeMet media, and used to start a new 50 mL culture. This second culture was grown to an OD_{600} of ~0.6 and used to inoculate the larger 1 L culture. The cells were grown at 37 °C to an OD_{600} of ~0.6; the temperature was then lowered to 25 °C, and the cells were induced with 500 μM IPTG. After an additional 10 h, the cells were spun down at 4420 × *g* for 10 min and stored at −80 °C.

The cells were resuspended in 10 mL of lysis buffer (50 mM potassium phosphate (KP_i), 300 mM NaCl, and 10 mM imidazole, pH 8.0) and broken using a sonicator. The clarified cell-free extract was adsorbed on a Ni-NTA column, and the column was washed with 6 column volumes of buffer containing 50 mM KP_i, 300 mM NaCl, and 10 mM imidazole, pH 8.0, and then eluted with 50 mM KP_i, 300 mM NaCl, and 250 mM imidazole, pH 8.0. The protein was then buffer-exchanged using an Econo-Pac 10DG column (BioRad) into 25 mM Tris, pH 7.6, concentrated to 30 mg/mL by ultrafiltration using a 3 kDa cutoff concentrator (Amicon), and stored at −80 °C. The protein concentration was determined by the Bradford method using bovine serum albumin as the standard. The purity of the thiazole synthase/ThiS complex was determined by Coomassie-stained SDS−PAGE and found to be 90−95% free from contaminating proteins (data not shown).

The E98A and D182A mutants were overexpressed and purified as described for the thiazole synthase/ThiS complex. The ThiF, ThiO, ThiD, ThiE, NifS, and YrvO proteins were all overexpressed as described previously (*3*) and stored in 50 mM Tris, pH 7.6, or 200 mM Tris, pH 7.8. DXP and [1-^{13}C]-DXP were synthesized as described previously (*4*).

Table 1: Data Collection Statistics[a]

	thiazole synthase/ThiS complex	
	peak (Se)	native
wavelength (Å)	0.9783	0.9783
resolution (Å)	25−3.4	25−3.15
no. of reflns	126 882	140 237
no. of unique reflns	14 776	20 101
redundancy	8.6 (8.3)	7.0 (6.8)
completeness	99.3 (99.7)	99.2 (100)
R_{sym}* (%)	12.8 (52.8)	11.2 (53.7)
I/σ	15 (3.8)	21 (2.18)

[a] Values for the outer resolution shell are given in parentheses. Data were collected at the Advanced Photon Source (APS) beam line 8BM. $R_{sym}* = \sum\sum_i |I_i - \langle I \rangle| / \sum \langle I \rangle$, where $\langle I \rangle$ is the mean intensity of the N reflections with intensities I_i and common indices h,k,l.

Crystallization of the Thiazole Synthase/ThiS Complex. The thiazole synthase/ThiS complex was crystallized using the hanging drop method with each drop containing 1 μL of protein and 1 μL of well solution. The well solution for optimized conditions contained 4%−6% poly(ethylene glycol) 8000 (PEG 8K), 200 mM sodium chloride, and 100 mM sodium phosphate, pH 6.0−6.2. Crystals appeared within 2 days and grew to their maximum size (0.08 mm × 0.08 mm × 0.5 mm) in 1 week. Preliminary X-ray analysis showed that the crystals belong to the space group $P6_122$ or $P6_522$ with unit cell dimensions of $a = 91.58$ and $c = 402.27$ Å. The crystals contain two thiazole synthase monomers and two ThiS monomers per asymmetric unit corresponding to a solvent content of 60%. The crystallization conditions for the native protein and SeMet incorporated protein were essentially the same except that 1 mM dithiothreitol (DTT) was added for the SeMet protein.

For cryoprotection, the crystals were gently transferred to a stabilization solution that was similar to the mother liquor but with 10% PEG 8K and 5% glycerol. The crystals were then transferred into solutions of increasing glycerol concentration (5% steps until the final concentration of 25% was reached) and frozen by plunging into liquid nitrogen and stored.

X-ray Data Collection and Processing. A single-wavelength data set was collected on a SeMet crystal at the Advanced Photon Source (APS) beam line 8-BM to 3.4 Å resolution. The wavelength was chosen to be at the maximum of the f'' (peak). The edge and remote wavelength data were not collected because of crystal decay. Data were collected over 40° using 60 s for each 1° oscillation with a crystal to Quantum 315 CCD detector (Area Detector Systems Corporation) distance of 450 mm. Bijvoet pairs were measured using inverse beam geometry in 10° wedges.

Single-wavelength data were also taken on a native crystal in a similar manner. In this case, data were collected over a range of 65° using 60 s for each 1.0° oscillation at a crystal to detector distance of 450 mm. Integration and scaling on both data sets were performed with HKL2000 (*10*). Data collection statistics are summarized in Table 1.

Structure Determination. The initial Se atom positions were determined utilizing Patterson search methods as implemented in SOLVE (*11*). An initial run found two of the possible 16 selenium sites. Using these as starting sites in a second iteration, the program found eight more sites. Their correctness was determined by a combination

of peak height and possession of a noncrystallographic 2-fold axis. The Se atom positions were input into CNS (*12*) and used for phasing. The initial phases were used to identify four of the six remaining Se atoms from a combination of anomalous difference Fourier and log-likelihood Fourier maps, and phases were recalculated using the 14 Se atom positions.

Model Building and Structure Refinement. All model building was performed using the computer program O (*13*). Electron density maps were calculated for each possible space group, $P6_122$ or $P6_522$; however, only the electron density for space group $P6_522$ showed features consistent with a protein structure. The map was further improved with the addition of noncrystallographic symmetry constraints generated from the initial selenium positions and a protein mask that was created from a bones representation of the electron density using the program MAPMAN (*14*). The electron density for one ThiS/thiazole synthase heterodimer was stronger than the other and was built first. The known structure of *E. coli* ThiS (PDB code 1F0Z) (*5*) was used as a guide for modeling the *B. subtilis* ThiS.

Following model building with the 3.4 Å Se phased map, the model in the asymmetric unit included two thiazole synthase monomers and one ThiS monomer. The thiazole synthase models included residues 1−43 and 60−234. Only one ThiS was clearly visible in the electron density, and the model included residues 1−64. Rigid body refinement, annealing, and *B*-factor refinement was performed with the 3.15 Å native data. Though the model was slightly improved, there were still sections of poor density near regions of missing residues.

The two thiazole synthase and one ThiS model was transferred to REFMAC5 (*15*) for continued refinement with TLS and NCS restraints. Sections of out-of-register residues became easily visible and were fixed. Successive rounds of model building, refinement, and map generation allowed for improvement of each of the models. In addition, density appeared more clearly for the final ThiS, and it was built in using the original ThiS as the model. Very strong unassigned density was built as a phosphate due to the shape of the density and the high levels of phosphate in the crystallization conditions.

The final model includes two thiazole synthase/ThiS complex heterodimers in the asymmetric unit with one bound phosphate in each. The more ordered ThiS/thiazole synthase dimer contains residues 1−242 of thiazole synthase and residues 1−65 of ThiS. The other thiazole synthase/ThiS dimer contains residues 1−141 and 148−243 of thiazole synthase and residues 1−64 of ThiS. The model also contains five water molecules that showed strong electron density and good hydrogen bonding geometry. The final refinement statistics are shown in Table 2.

Competitive Binding of ThiS to ThiF and Thiazole Synthase. Aliquots (50 mL) of the thiazole synthase/ThiS complex overexpression strain (His-tag on ThiS) were mixed with increasing volumes of the ThiF overexpression strain (0, 50, 100, 150, and 200 mL). The resulting mixed cultures were lysed. The His-tagged ThiS and its associated proteins (non-His-tagged ThiF or thiazole synthase) were purified using NTA affinity chromatography on a Qiagen spin column and analyzed by SDS−PAGE (4−20% gradient gel BIO-RAD) with Coomassie staining.

Table 2: Refinement Statistics

	APS (8BM) native
resolution (Å)	15−3.15
total no. of non-hydrogen atoms	4556
no. of protein atoms	4541
no. of water oxygens	5
no. of ligand atoms	10
no. of reflns in refinement	15 975
no. of reflns in test set	1261
R factor[a] (%)	24.2
R_{free}[b] (%)	30.5
rms deviation from ideal geometry	
bonds (Å)	0.022
angles (deg)	2.02
Ramachandran plot	
most favored region (%)	77.9
additional allowed region (%)	18.5
generously allowed region (%)	2.9
disallowed region (%)	0.8
average *B*-factors (Å^2)	
protein	45.6
water	88.9
ligand	26.5

[a] R factor $= \sum_{hkl}||F_{obsd}| - k|F_{calcd}||/\sum_{hkl}|F_{obsd}|$, where F_{obsd} and F_{calcd} are observed and calculated structure factors, respectively. [b] For R_{free}, the sum is extended over a 7% subset of reflections excluded from all stages of refinement.

Trapping of the Thiazole Synthase/ThiS/DXP Imine Complex by Borohydride Reduction. [1-^{13}C]-DXP (150 μM) in 200 μL of 50 mM Tris-HCl, pH 7.6, containing the ThiS/thiazole synthase complex (2 mg/mL) was incubated at room temperature for 2 h. The reaction mixture was then treated with $NaBH_4$ (400 mM) for 20 min. Foaming was controlled by spinning the reaction mixture in a clinical centrifuge. One hundred microliters of this solution was gel filtered using a Biospin column (BIO-RAD Tris, pH 7.4, 0.02% NaN_3) to remove excess DXP and boron salts. The resulting protein solution was frozen and stored at −80 °C until further use. An identical trapping protocol was followed for the E98A and D182A thiazole synthase mutants.

ESI-FTMS Analysis of the Trapped Thiazole Synthase/ThiS/DXP Imine. Protein samples were desalted using reverse-phase protein traps (Michrom Bioresources, Auburn, CA), washed with MeOH/H_2O/AcOH (1:98:1), and eluted with MeOH/H_2O/AcOH (70:26:4). The desalted proteins were electrosprayed at 1−50 nL/min with a nanospray emitter. The resulting ions were guided through a heated capillary, skimmer, and three radio frequency-only quadrupoles into a 6 T modified Finnigan FTMS with the Odyssey data system (*16*).

Thiazole Synthase Catalyzed Sulfur Transfer from [^{35}S]-ThiS−Thiocarboxylate. [^{35}S]-ThiS−thiocarboxylate was prepared by incubating the following reaction mixture at room temperature for 80 min (all in 200 mM Tris, pH 7.8) followed by gel filtration using a Biospin column into 0.02% NaN_3, 25 mM Tris, pH 7.4: 30 μL of [^{35}S]-cysteine stock (prepared using 9 μL (50 μCi) of [^{35}S]-cysteine in 90 μL of 2 mM cysteine and 4 mM DTT, in 200 mM Tris, pH 7.8), 2 μL of 200 mM ATP, 1 μL of 800 mM $MgCl_2$, 25 μL of thiazole synthase/ThiS (15 mg/mL), 5 μL of ThiF (8 mg/mL), and 5 μL of NifS (2 mg/mL) to give a total of 68 μL of solution. DXP (1 μL of a 12.5 mM solution) was added to 30 μL of this protein sample, followed 8 min later by 5 μL of freshly prepared 1 M $NaBH_4$. After 20 min, 40 μL of 2× SDS−

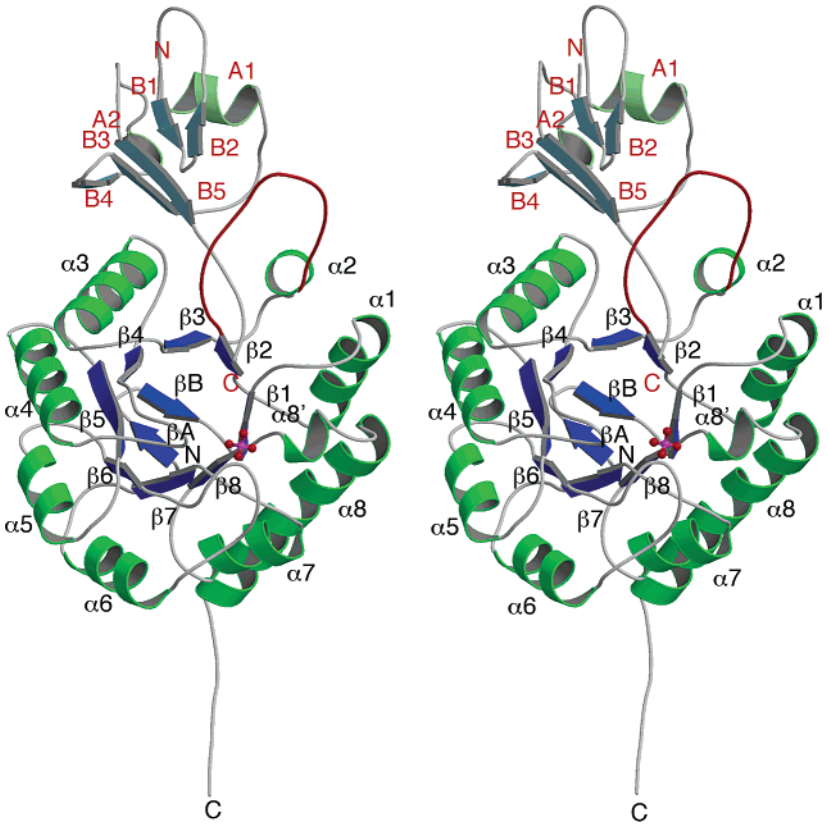

FIGURE 1: Structure of the thiazole synthase/ThiS complex. Stereoview of the thiazole synthase/ThiS heterodimer is drawn in ribbon representation. The bound phosphate is shown in ball-and-stick representation. ThiS is labeled in red with α-helices labeled A# and β-strands labeled B#. Thiazole synthase is labeled in black with α-helices labeled α# and β-strands labeled β#. Secondary structural elements are colored green for α-helices and blue for β-strands. The "clamp" loop that mediates ThiS binding to thiazole synthase is colored in red. This figure was prepared with Molscript (*29*) and Raster3D (*30*).

PAGE buffer was added. Reaction mixtures using the E98A and D182A thiazole synthase mutants and control reactions from which DXP was omitted were prepared in a similar fashion. These six samples were then analyzed by 15% SDS−PAGE. The developed gel was washed thoroughly with water and dried in vacuo between gel drying film (Promega) using a BIO-RAD gel dryer (model 583). The dried gel was exposed to biomax MR (Kodak) autoradiography film for 5 days at −80 °C, and the film was developed using Kodak GBX developer and replenisher, washed with distilled water, fixed using Kodak GBX fixer and replenisher, and again thoroughly washed with distilled water before drying.

Assay for Thiazole Synthase Catalyzed Thiazole Phosphate Formation. The thiazole phosphate synthase activity of the wild-type enzyme and both the E98A and D182A mutants was determined as described previously (*3*).

Thiazole Synthase Catalyzed H/D Exchange of the C3 Proton of DXP. Deuterated buffer was prepared by lyophilizing 2.5 mL of 400 mM KP_i (pH 7.6) and dissolving the resulting solid in 100 mL of D_2O. This was used to equilibrate a PD-10 gel filtration column. Purified thiazole synthase/ThiS was buffer-exchanged into deuterated buffer (10 mM KP_i, pH 7.6) using this column. The buffer-exchanged protein was collected in 0.5 mL fractions. The two most concentrated fractions (total 1 mL) were used for the assay (protein concentration is ~5 mg/mL).

DXP (1 mM) was added to 1 mL of the purified, buffer-exchanged protein. After 15 min at room temperature, the reaction mixture was cooled to 4 °C and filtered through a 3 kDa membrane prewashed with D_2O (Microcon, 6370 × *g*). The filter was again washed with D_2O (500 μL). The second washings and the filtered reaction mixture were combined, lyophilized, redissolved in 600 μL of D_2O, and analyzed by ^1H NMR. The mutants were analyzed in an identical manner, and a control reaction from which the enzyme was omitted was also run.

Modeling of DXP into the Active Site of Thiazole Synthase. DXP was modeled into the active site of thiazole synthase using the program PRODRG2 (*17*) and the following four constraints: (1) the C2 carbon of DXP was bound to Lys98; (2) the phosphate moiety of DXP was placed in the phosphate site; (3) a glycine thiocarboxylate was added to ThiS; (4) this thiocarboxylate was covalently attached to the C3 carbon of DXP giving a tetrahedral intermediate. Active site residues of ThiS and thiazole synthase were manually adjusted to minimize bad contacts and to maximize hydrogen bonds within the context of the other constraints.

RESULTS

Description of the Structure of the Thiazole Synthase/ThiS Complex. The thiazole synthase monomer adopts a classic $(\beta\alpha)_8$ barrel fold with a few minor additions (Figure 1). A two-stranded antiparallel β-sheet (βA−βB) precedes the initial beta strand (β1) and caps the N-terminal face of the barrel. In addition, helix α8′ is inserted between β8 and α8. Finally, there is a 14 residue loop between β2 and α2, and α2 is shortened to one turn.

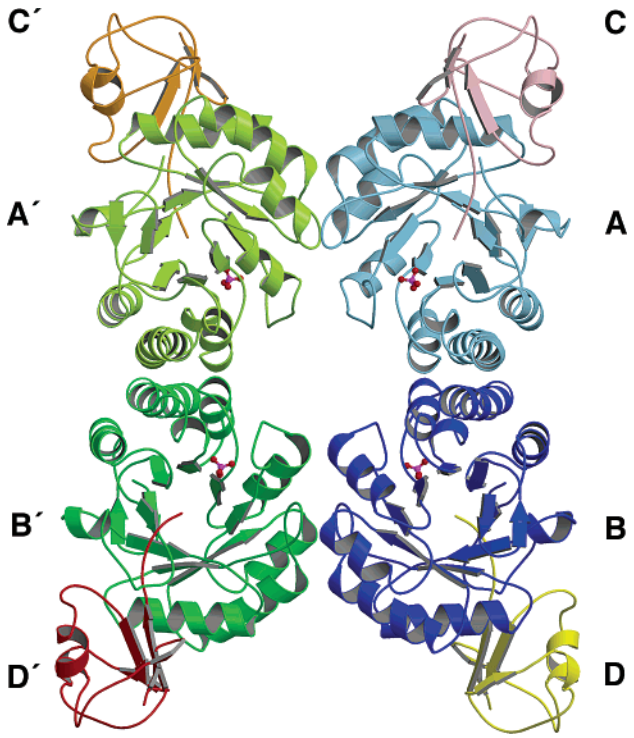

FIGURE 2: Structure of the thiazole synthase/ThiS complex. The view is down the noncrystallographic 2-fold axis. The crystallographic 2-fold axis is vertical, and the second noncrystallographic 2-fold axis is horizontal. Phosphate is shown bound in ball-and-stick representation. Thiazole synthase monomers (A, B, A′, and B′) are colored in blues and greens. ThiS monomers (C, D, C′, and D′) are colored pink, orange, yellow and red. This figure was prepared with Molscript (*29*) and Raster3D (*30*).

ThiS has a compact fold consisting of a four-stranded mixed β-sheet flanked on one side by two short α-helices (Figure 1). Hydrophobic interactions dominate interactions between the α-helices and the β-sheet. The C-terminal tail extends outward from the core of the structure and the final C-terminal glycine residue is missing in the model due to poor density most likely a result of high flexibility of the tail. ThiS from *B. subtilis* shares 21% identity to *E. coli* ThiS. Superposition of the X-ray structure of ThiS from *B. subtilis* and the NMR structure from *E. coli* shows an rmsd of 2.9 Å in Cα atom positions for 62 out of 66 residues. ThiS also shares significant structural similarity with ubiquitin (rmsd of 2.9 Å for 57 of 76 residues with 12% identity) (*18*) and MoaD (rmsd of 2.8 Å for 58 of 81 residues with 21% identity) (*19*).

Quaternary Structure. Thiazole synthase is a tetramer with 222 point symmetry and has a rectangular box shape with dimensions 85 Å × 75 Å × 35 Å (Figure 2). The molecular weight of the complex based on gel filtration analysis is 156 kDa, consistent with a tetramer in solution (unpublished results). Monomers A and A′ (B and B′) are related by the crystallographic 2-fold axis, while the other pairs of monomers are related by noncrystallographic 2-fold axes. A channel parallel to one of the noncrystallographic 2-fold axes, and approximately parallel to the crystallographic *c* axis, is formed at the center of the thiazole synthase tetramer by the C-terminal tail, the β6-α6 loop, α6, and α7 of each monomer. The axes of the β-barrels of the thiazole synthase monomers are also approximately parallel to the channel axis. The ThiS binding sites, which are located at the C-terminal faces of the thiazole synthase β-barrels, alternate in an up/down arrangement with the active sites for monomers A and B′ above the tetramer and A′ and B below the tetramer as viewed in Figure 2.

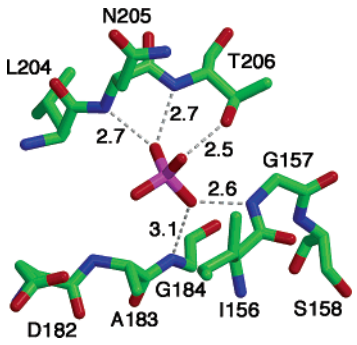

FIGURE 3: View of the phosphate binding site. A stick representation of the phosphate binding site with residues labeled with their one letter designation is presented. Hydrogen bonds to the phosphate are shown in a dashed gray line labeled with distances given in angstroms. This figure was prepared with Molscript (*29*) and Raster3D (*30*).

The main interactions between monomers A and B are hydrophobic contacts that occur between helix α7 and helix α8 of monomer A to the 2-fold related helices in monomer B. In addition, there is an extended structure for the C-terminal tail of each monomer that interacts with helix α8′ and the β6/α6 loop of the other monomer. These interactions bury roughly 14% of the total available surface area and also include 10 hydrogen bonds. The interface between monomers A and A′ is dominated by 2-fold related hydrophobic areas formed between the β4-α4 loop with helices α5 and α6 of the related monomer. In addition, 2-fold related pairs of helix α4 form a separate hydrophobic interaction. These interactions bury 8.5% of the total accessible surface area and also include eight hydrogen bonds and four salt bridges. Finally, Tyr242 in the C-terminal tail of monomer A forms a herringbone stacking interaction with Phe170 from helix α6 of monomer B′.

Thiazole Synthase/ThiS Interactions. There are two main areas of interaction between thiazole synthase and ThiS. The first area, called the "clamp" loop, is dominated by hydrophobic contacts and involves the extended 14 residue β2−α2 loop of thiazole synthase. The C-terminal tail of ThiS is inserted through this loop much like a thread through the eye of a needle. Hydrophobic residues on this loop, Met45, Ile46, and Phe47, pack against the slightly exposed conserved hydrophobic interior of ThiS between the ThiS β-sheet and helix α1. The second area is also dominated by hydrophobic contacts and involves conserved surface hydrophobic residues on β3, β4, and β5 of ThiS with hydrophobic residues on β1, α1, β2, α2, α3, and the α3−β4 loop of thiazole synthase. The main interactions are hydrophobic; however, there are three salt bridges and 11 hydrogen bonds with a total of ∼10% of the thiazole synthase accessible surface area buried by ThiS.

Phosphate Binding Site. A phosphate ion was unambiguously observed in the electron density in the expected active site region and is assumed to occupy the phosphate binding site of DXP. The phosphate ion makes hydrogen bonding interactions with residues from helix α8′, the β7−α7 loop, and the β6−α6 loop (Figure 3). The phosphate forms hydrogen bonds with the backbone nitrogen atoms of Gly157,

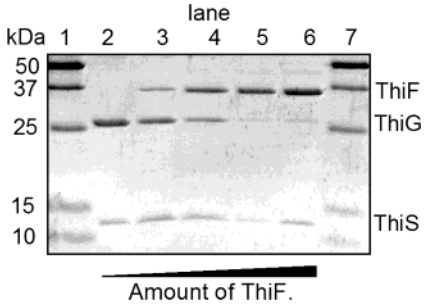

FIGURE 4: Coomassie-stained 4−20% SDS−PAGE of thiazole synthase (ThiG) and ThiF copurification with ThiS: lane 1, molecular weight markers; lane 2, NTA-purified ThiS/ThiG (50 mL culture); lane 3, NTA-purified ThiS/ThiG (50 mL culture) in the presence of 50 mL of the ThiF culture; lane 4, NTA-purified ThiS/ThiG (50 mL culture) in the presence of 100 mL of the ThiF culture; lane 5, NTA-purified ThiS/ThiG (50 mL culture) in the presence of 150 mL of the ThiF culture; lane 6, NTA-purified ThiS/ThiG (50 mL culture) in the presence of 200 mL of the ThiF culture; lane 7, molecular weight markers. In each case, ThiS was His-tagged.

Table 3: Quantitation of Thiazole Phosphate Formation

	time (min)	amount of thiazole phosphate (nmol)	activity (pmol/min)	relative rate
WT	15	1.7	113	100
E98A	120	0.35	2.9	2.6
D182A	120	*a*	*b*	0

[a] Not detected (<0.10 nmol). [b] Not detected (<0.8 pmol/min).

Gly184, Asn205, and Thr206 and with Oγ1 of Thr206. Of these residues, Gly157 and Gly184 are conserved and Thr206 is always threonine or serine.

ThiF/Thiazole Synthase Competition Assay. The thiazole synthase complexed to His-tagged ThiS was purified by Nickel-NTA chromatography in the presence of increasing concentrations of ThiF and analyzed by SDS−PAGE. As the concentration of ThiF increased, the amount of thiazole synthase that copurified with ThiS decreased indicating that ThiF and thiazole synthase compete for a common binding site on ThiS (Figure 4).

Effect of the D182A and E98A Thiazole Synthase Mutants on Thiazole Phosphate Formation. The D182A and E98A thiazole synthase mutants were assayed for thiazole phosphate synthase activity by converting the biosynthesized thiazole phosphate to the highly fluorescent thiochrome phosphate as previously described (*3*). The E98A mutant was approximately 38-fold less active than the native enzyme, and the D182A mutant was inactive (>140-fold reduction, Table 3).

Imine Formation Catalyzed by the D182A and E98A Thiazole Synthase Mutants. Native and the E98A and D182A mutants of thiazole synthase were incubated with DXP followed by reduction of the DXP−thiazole synthase imine with borohydride as previously described (*4*). ESI-FTMS analysis of the resulting proteins indicated that both the D182A and E98A mutants formed stable adducts with an extra 200 Da demonstrating that these thiazole synthase mutants are able to catalyze imine formation with DXP (Figure 5). The rate of imine formation was not decreased by more than 25% for either mutation (unpublished results).

Thiazole Synthase Catalyzed Sulfur Transfer from [^{35}S]-ThiS−Thiocarboxylate. The sulfur transfer from [^{35}S]-ThiS−thiocarboxylate to thiazole synthase was monitored by SDS−PAGE/autoradiography as previously described (*20*) (Figure 6). The radioactivity incorporated into the thiazole synthase E98A mutant was 15-fold less than that in the native enzyme, and the D182A mutant was inactive.

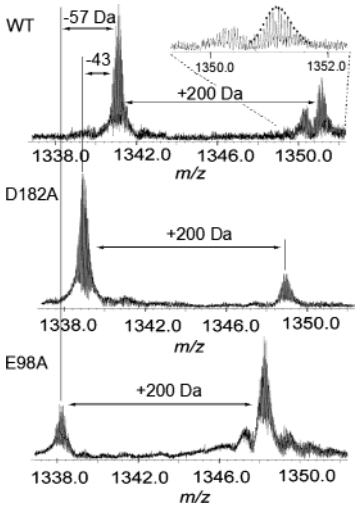

FIGURE 5: The effect of thiazole synthase E98A and D182A mutations on imine formation. The top panel shows $NaBH_4$-reduced thiazole synthase (WT)/DXP imine. The region for *m*/*z* 1349.8−1352.2 is enlarged. The theoretical molecular weight for reduced thiazole synthase + DXP is indicated by the black circles (●). The middle panel shows $NaBH_4$-reduced thiazole synthase (D182A)/DXP imine. The bottom panel shows $NaBH_4$-reduced thiazole synthase (E98A)/DXP imine. Reduction of the DXP imine ($C_5H_{13}PO_6$) resulted in a mass increase of 200 Da.

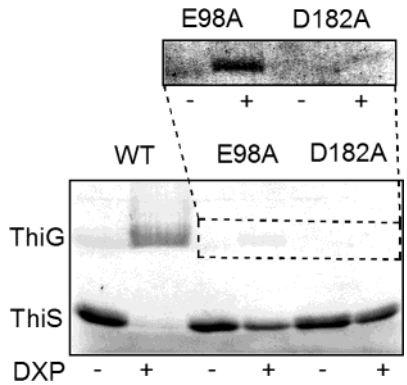

FIGURE 6: Analysis of the sulfur transfer from [^{35}S]-ThiS−thiocarboxylate to the thiazole synthase(ThiG)/DXP imine for native and mutated thiazole synthase.

Thiazole Synthase Catalyzed H/D Exchange of the C3 Proton of DXP. The thiazole synthase catalyzed exchange of the C3 proton of DXP can be readily monitored by NMR. Figure 7 shows the partial NMR spectrum of DXP (C3 and C4 protons). The C3 proton is completely exchanged with retention of stereochemistry by the native enzyme. In contrast, under identical conditions, the E98A mutant catalyzed partial exchange at C3, while the D182A mutant showed no exchange. This suggests that Asp182 may be the base involved in the deprotonation of the C3 carbon of DXP during thiazole formation.

DISCUSSION

Comparison of Thiazole Synthase to Related Proteins. A structural search using DALI (*21*) indicated that among the 21 homologous superfamilies of $(\beta\alpha)_8$ barrels, thiazole

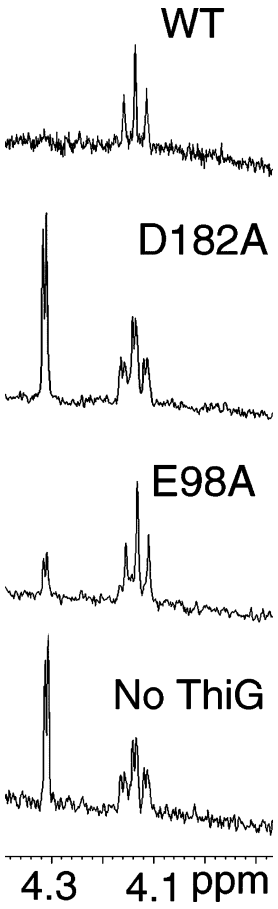

FIGURE 7: NMR analysis of the proton exchange at C3 of DXP catalyzed by native and mutated thiazole synthase.

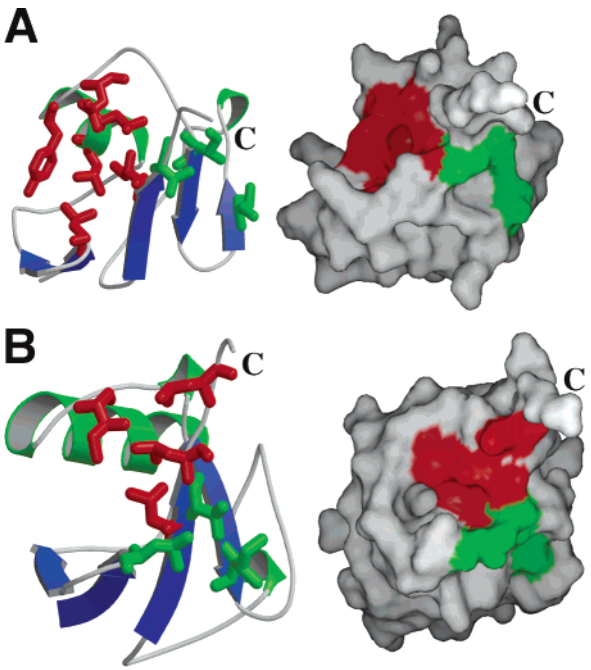

FIGURE 8: ThiS and ubiquitin surface hydrophobic pockets. Panel A presents ThiS drawn in ribbon representation with α-helices in green and β-strands in blue. Residues from the commonly used conserved hydrophobic binding pocket are shown in green. Residues from the alternate conserved hydrophobic binding pocket are shown in red. Panel B presents ubiquitin drawn in ribbon representation colored as described for ThiS in panel A. Residues are also colored as described in panel A. This figure was prepared with Molscript (*29*) and Raster3D (*30*).

synthase is most closely related to the FMOP superfamily. These DALI results showed that the top 20 structural alignments to thiazole synthase are dominated by proteins from the FMOP superfamily, which is characterized by a conserved phosphate binding pocket consisting of residues from β6, β7, and α8′. Interestingly, one of the top alignments of thiazole synthase was to the FMOP superfamily member *B. subtilis* thiamin phosphate synthase with an rmsd of 2.5 Å for 185 of 226 residues.

Thiazole synthase also aligns well with fructose 1,6-(bis)-phosphate aldolase class 1A (FBPA 1A) from the archaea *Thermoproteus tenax* (TtFBPA) (*22*) with an rmsd of 3.4 Å for 185 of 250 residues. Class 1 aldolases (ALD1) are generally eukaryotic in origin and form a Schiff base intermediate with an active site lysine to reversibly cleave fructose 1,6-(bis)phosphate to glyceraldehyde phosphate and dihydroxyacetone phosphate. Class 2 aldolases (ALD2) are generally from bacteria and do not utilize a Schiff base in their reaction mechanisms. TtFBPA is unique in the ALD1 family since it is archaeal in origin. It has been suggested that TtFBPA represents an evolutionary link between the ALD1 and ALD2 families (*23*).

The imine-forming lysine in the ALD1 family is generally located on strand β6 of the barrel. On the other hand, the active site lysine of thiazole synthase is located on strand β4. However, when structurally aligned, the amino groups of the active site lysines closely overlap. The functional conservation of the lysine, along with the structural conservation of several salt bridges throughout the barrel, suggests an evolutionary relationship between thiazole synthase and the ALD1 family of proteins.

Transaldolase B is a unique member of the ALD1 family in that, like thiazole synthase, its active site lysine is on strand β4 of the barrel. However, it has previously been suggested through structural alignments that transaldolase B evolved from a circular permutation in an ancestral aldolase gene, which results in strand β4 aligning with strand β6 of a traditional aldolase (*24*). Thiazole synthase is unique in that, like transaldolase B, its active site lysine is located on strand β4; however, it structurally aligns with the ALD1 family in which the active site lysine is on strand β6.

Previously, it has been suggested through structural and sequence alignments among all the $(\beta\alpha)_8$ barrel superfamilies that the FMOP family should also include the ALD1 family. The structure of thiazole synthase is consistent with a common evolutionary origin of these two families. Furthermore, the relationship of thiazole synthase to TtFBPA suggests that the ALD2 family may also share this common ancestor.

Thiazole Synthase/ThiS Binding Motifs. The thiazole synthase/ThiS interface is 62% hydrophobic, utilizing three main hydrophobic surfaces: the main ThiS β-sheet near the C-terminal tail, the C-terminal tail, and the exposed hydrophobic patch between α1 and the interior portion of the β-sheet (Figure 8A). In addition, three salt bridges form between Glu58, Glu35, and Lys30 on ThiS with Arg44, Arg81, and Glu159 on thiazole synthase, respectively. Of these residues, only Arg44 is absolutely conserved, whereas Glu58 is generally either a glutamate or an aspartate. The interface also contains 11 hydrogen bonds.

Table 4: Protein Systems Related to Thiazole Biosynthesis

pathway	ubiquitin homolog	activating enzyme (E1 homolog)	conjugating enzyme/synthase (E2 homolog)
thiamin biosynthesis	ThiS	ThiF	ThiG
molybdopterin biosynthesis	MoaD	MoeB	MoaE
protein degradation	ubiquitin	UBA1 (E1)	UBC (E2)
E3 ligase regulation	NEDD8	APPBP1-UBA3 (E1)	UBC12 (E2)

Evolutionary relationships have been proposed for MoaD, ubiquitin/ubls, and ThiS and the enzymes with which they interact (*5*) (Table 4). The structures of MoaD (*7*) and NEDD8 (*8*) with their activating proteins, MoeB and APPBP1-UBA3, respectively, showed that protein−protein interactions may also be conserved. Evaluation of the thiazole synthase/ThiS interface reveals features similar to the interfaces of related systems. ThiS contains a highly conserved hydrophobic binding patch (residues Ile33, Ile40, and Val60) on the β-sheet near the C-terminal tail that is structurally homologous to the Leu71, Leu73, and Ile36 hydrophobic patch found on ubiquitin (Figure 8B) and a similar one found on MoaD. This patch forms protein−protein interactions in the thiazole synthase/ThiS complex and serves a similar role in complexes of ubls with their respective E1-like proteins (*8*). In addition, the molybdopterin synthase structure further supports the importance of this hydrophobic patch (*19*).

The C-terminal tails of ThiS, MoaD, and ubiquitin/ubls also provide key binding partner interactions. In the case of thiazole synthase, residues Phe62 and Val63 of ThiS and Phe142, Leu148, and Leu158 of thiazole synthase form conserved hydrophobic interactions that orient the C-terminal tail of ThiS in the thiazole synthase active site. Studies on NEDD8, a ubl, and ubiquitin have shown that a single mutation in their C-terminal tails can alter the specificity of a cognate E1 for its ubl (*25*, *26*).

The final area of ThiS that contains key hydrophobic interactions is unique among all known ubl complex structures. This hydrophobic surface patch is found between the C-terminal tail of ThiS and the interior side of thiazole synthase helix α1 (Figure 8). Here a conserved hydrophobic patch is composed of Leu4, Leu21, Leu22, Tyr25, Leu27, and Ile59. Thiazole synthase makes hydrophobic interactions with the "clamp" loop using residues Ile47 and Phe48. There are two additional interactions that mediate the binding of the "clamp" loop to ThiS. The absolutely conserved Asn4 of ThiS hydrogen bonds to both the backbone oxygen of Met46 on the "clamp" loop and the backbone nitrogen of Ile59 of the C-terminal tail. Also, Lys30 on ThiS forms a salt bridge with Glu57 on the α2 helix of thiazole synthase near the bottom of the "clamp" loop.

The hydrophobic patch on ThiS involved in "clamp" loop binding can also be found on the surface of ubiquitin and NEDD8 but to a lesser extent on MoaD. NEDD8 and ubiquitin have a homologous hydrophobic patch involving residues Ile36, Leu69, and Leu71. The structures of uncomplexed NEDD8 and NEDD8 bound to its E1, APPBP1-UBA3, reveal that this hydrophobic area decreases slightly upon E1 binding (*8*, *25*). Furthermore, the complex of

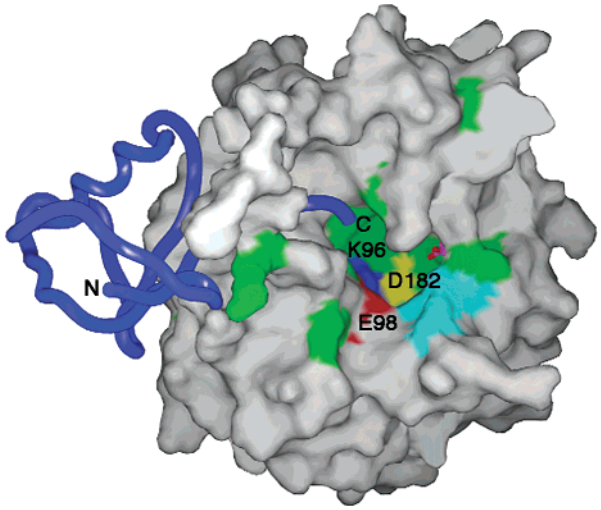

FIGURE 9: Putative active site of thiazole synthase. Thiazole synthase is shown as a surface representation, and ThiS is shown as a blue coil. Conserved residues with predicted functions are shown: Lys96 (blue), Glu98 (red), and Asp182 (yellow). Conserved residues without an assigned function are colored in green, and an exposed hydrophobic surface is colored in cyan. Phosphate is shown in red ball-and-stick representation. This figure was prepared with SPOCK (*31*).

NEDD8−E1 indicates that many of these residues are only slightly buried though generally not in hydrophobic areas. Leu69, in particular, is in the center of the hydrophobic patch, and yet it has no interactions with either of the other proteins. Instead, most protein−protein interactions of NEDD8 to E1 are through the two previous binding areas, as well as through the more polar surface area on the opposite side of α1.

MoaD, on the other hand, maintains this hydrophobic binding patch despite significant structural differences from ThiS, NEDD8, and ubiquitin. MoaD, in comparison to the other three proteins, has two extra α-helices: one between β1 and β2 designated α1′ and one between α1 and β3 designated α2. In this case, α1′ and α2 form in the place of the hydrophobic patch and block surface access to the hydrophobic interior of the protein. Surprisingly, despite these differences in structure, this region contains a similar hydrophobic patch, including residues Val10, Leu13, Leu44, Pro76, and Leu51. However, neither the molybdopterin synthase complex nor the MoaD−MoeB complex utilize this binding area for complex stabilization (*7*, *19*).

Overall, the evolutionary conservation of this hydrophobic binding patch across structurally similar proteins suggests the potential for uncharacterized protein−protein interactions that utilize the area. For example, the structure of the complex between NEDD8 and its conjugating enzyme, UBC12, has yet to be determined.

ThiF and Thiazole Synthase Bind to the Same Surface of ThiS. ThiF has a high sequence similarity (>50%) to both MoeB and E1-like proteins. The sequence similarity of the activating proteins and the structural similarity of ThiS and MoaD (*5*) suggest that the ThiS/ThiF and MoeB/MoaD complex will also be similar. However, thiazole synthase does not have a high sequence identity to either MoaE, or any E2, so the relationship between the thiazole synthase/ThiS and MoaE/MoaD complexes was unclear. The thiazole synthase/ThiS structure indicates that the same surface that has been suggested to be involved in ThiS/ThiF complex

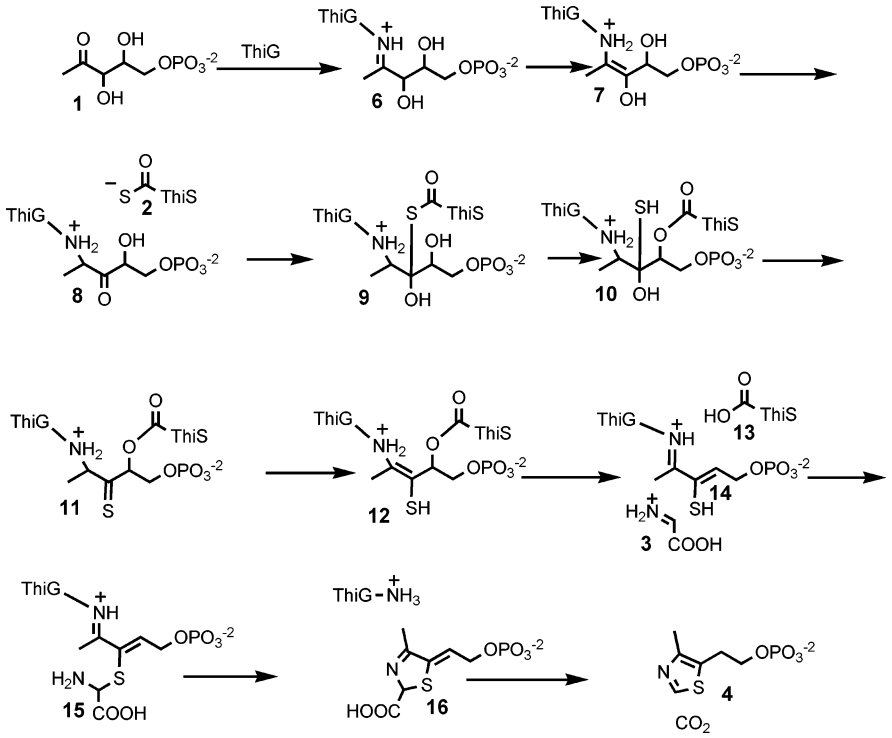

FIGURE 10: Mechanistic proposal for the thiazole synthase (ThiG) catalyzed formation of the thiazole moiety of thiamin pyrophosphate.

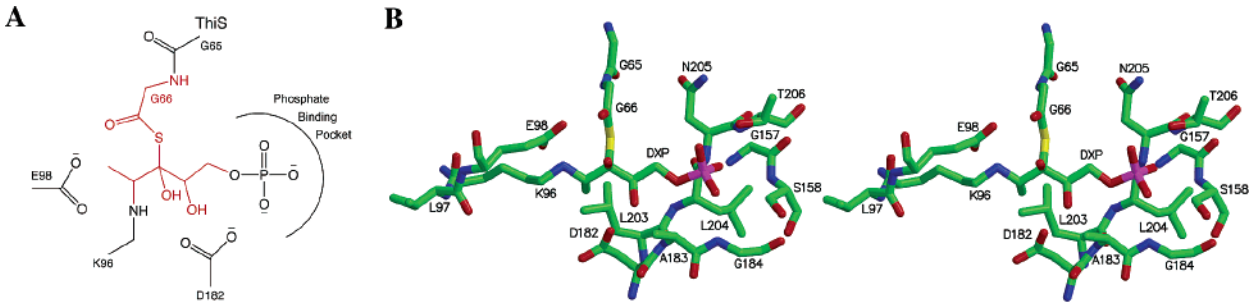

FIGURE 11: Model of DXP bound to the thiazole synthase active site. Panel A presents a schematic representation showing DXP and key amino acid side chains. Atoms shown in black were observed experimentally, and atoms shown in red were modeled using structural and mechanistic information. Panel B presents a stereoview of the model of DXP bound to the thiazole synthase/ThiS complex. This figure was prepared with Molscript (*29*) and Raster3D (*30*).

formation (*19*) is involved in thiazole synthase/ThiS complex formation. Thus, despite the structural difference of thiazole synthase to either MoaE or E2-like proteins, a common binding motif is used for complex formation of ThiS, MoaD, and ubiquitin with their respective enzyme partners. To support this hypothesis, we were able to show that ThiF competes with thiazole synthase for ThiS binding (Figure 4).

Identification of the Thiazole Synthase Active Site. The location of the thiazole synthase active site was deduced on the basis of several factors (Figure 9). First, the face of a $(\beta\alpha)_8$ barrel corresponding to C-terminal ends of the β-strands generally contains the active site, and in thiazole synthase, this region contains most of the absolutely conserved residues. Similar binding sites are found in thiamin phosphate synthase (*27*) and fructose 1,6-(bis)phosphate aldolase (FBPA) (*28*), both $(\beta\alpha)_8$ barrels. Second, a phosphate ion was found bound to a region that contained a cluster of highly conserved residues. Third, Lys96, which forms an imine with DXP, is found close to the phosphate binding site. Fourth, the C-terminal tail of ThiS extends into the region of thiazole synthase where both Lys96 and the phosphate binding site are found. The phosphate of DXP most likely binds in a similar way as the bound phosphate in the current structure. Several absolutely conserved residues form this binding site. The phosphate binding site contains a P-loop similar to the one found in thiamin phosphate synthase for the binding of the phosphate of its substrate.

Active Site Model and E96A and D182A Mutagenesis. A mechanistic proposal for the formation of the thiazole phosphate moiety of thiamin pyrophosphate is outlined in Figure 10. In this proposal, DXP (**1**) forms an imine with Lys96 of the thiazole synthase. This tautomerizes first to the enamine **7** and then to the aminoketone **8**. Addition of ThiS−thiocarboxylate (**2**) followed by a S/O acyl shift gives intermediate **10**. Loss of water from **10** followed by tautomerization gives thioenol **12**, which eliminates ThiS−carboxylate to give **14**. Addition of the thiol of **14** to dehydroglycine (**3**) followed by transimination and decarboxylation reactions completes the thiazole biosynthesis. This mechanistic proposal has substantial experimental support (*3*, *4*, *20*). The thiazole synthase−DXP imine (**6**) has been trapped and characterized, thiazole synthase catalyzed exchange of the C3 proton of DXP with water has been

detected, and it has been demonstrated that one of the carboxy-terminal oxygen atoms of ThiS−carboxylate (**13**) is derived from DXP and not from the buffer. In addition, the intermediate **14** has been trapped and characterized as a competent sulfur donor for thiazole formation after the addition of dehydroglycine (**3**) (Dorrestein, P. C., Zhai, H., McLafferty, F., and Begley, T. P., *Chem. Biol.*, in press. This mechanistic proposal, combined with the structure of thiazole synthase complexed to the sulfur carrier protein, enables us to further elucidate the catalytic mechanism of this complex reaction sequence.

Based on the rationale that DXP binding is restricted by the position of lysine 96, the phosphate binding site, and the carboxy terminus of ThiS−carboxylate, intermediate **9** was modeled into the potential active site (Figure 11). This model was surprising in its simplicity; the residues likely to participate in catalysis were Glu98 and Asp182. Glu98 was near the C2 of DXP, and Asp182 was near C3 and C4 of DXP (Figure 11). Both of these residues are absolutely conserved. However, because of the approximate nature of our active site model and the complexity of the catalyzed reaction, it was not possible to assign specific functions to Asp182 and Glu98, and the catalytic function of these residues was therefore explored by mutagenesis.

The E98A mutant showed a 38-fold reduction in thiazole phosphate production, while the D182A mutant was inactive (>140-fold reduction, Table 3) confirming the importance of these residues in the biosynthesis of thiazole phosphate. Next we looked at the ability of the E98A and D182A mutants to catalyze the sulfur transfer from ^{35}S−ThiS thiocarboxylate to the aminoketone **8** to give **14**, which could be detected by SDS−PAGE/autoradiography after borohydride trapping (Figure 6). In this experiment, the D182A mutant was unable to catalyze the sulfur transfer reaction while the E98A mutant showed only weak catalytic activity (Figure 6). To further narrow down the catalytic roles of these residues, we looked at the ability of the mutants to catalyze the exchange of the C3 proton of DXP with water (Figure 7). This experiment demonstrated that the E98A mutant catalyzed the proton exchange, while the D182A mutant was inactive. This allows us to assign one of the functions of Asp182 to the deprotonation at C3 of the imine **6**. We have also examined the ability of the two mutants to catalyze the formation of imine **6** (Figure 5). Both mutants catalyze imine formation (unpublished results) with rates that are essentially the same as the rates of the native enzyme suggesting that neither residue plays an important role in the catalysis of imine formation. While these studies clearly identify one of the functions of Asp182, mutagenesis is of limited value in probing the functional roles of amino acids that participate in the catalysis of a complex multistep process where single amino acids are likely to have multiple roles. Further elucidation of these roles must await the solution of thiazole synthase structures with active site bound intermediates.

ACKNOWLEDGMENT

We thank Leslie Kinsland for assistance in the preparation of this manuscript. We thank NE-CAT beam line 8-BM, supported by NIH Grant RR15301, for providing synchrotron beam time. We thank Cynthia Kinsland at the Cornell Protein Purification Facility for the preparation of the thiazole synthase (E98A)/ThiS, the thiazole synthase (D182A)/ThiS, and the ThiF overexpression plasmids used in this study.

REFERENCES

1. Begley, T. P., Downs, D. M., Ealick, S. E., McLafferty, F. W., Van Loon, A. P., Taylor, S., Campobasso, N., Chiu, H. J., Kinsland, C., Reddick, J. J., and Xi, J. (1999) Thiamin biosynthesis in prokaryotes, *Arch. Microbiol. 171*, 293−300.
2. Settembre, E., Begley, T. P., and Ealick, S. E. (2003) Structural biology of enzymes of the thiamin biosynthesis pathway, *Curr. Opin. Struct. Biol. 13*, 739−747.
3. Park, J. H., Dorrestein, P. C., Zhai, H., Kinsland, C., McLafferty, F. W., and Begley, T. P. (2003) Biosynthesis of the thiazole moiety of thiamin pyrophosphate (vitamin B1), *Biochemistry 42*, 12430−12438.
4. Dorrestein, P. C., Huili Zhai, H., Taylor, S. V., McLafferty, F. W., and Begley, T. P. (2004) The biosynthesis of the thiazole phosphate moiety of thiamin (vitamin B(1)): the early steps catalyzed by thiazole synthase, *J. Am. Chem. Soc. 126*, 3091−3096.
5. Wang, C., Xi, J., Begley, T. P., and Nicholson, L. K. (2001) Solution structure of ThiS and implications for the evolutionary roots of ubiquitin, *Nat. Struct. Biol. 8*, 47−51.
6. Xi, J., Ge, Y., Kinsland, C., McLafferty, F. W., and Begley, T. P. (2001) Biosynthesis of the thiazole moiety of thiamin in *Escherichia coli*: identification of an acyl disulfide-linked protein−protein conjugate that is functionally analogous to the ubiquitin/E1 complex, *Proc. Natl. Acad. Sci. U.S.A. 98*, 8513−8518.
7. Lake, M. W., Wuebbens, M. M., Rajagopalan, K. V., and Schindelin, H. (2001) Mechanism of ubiquitin activation revealed by the structure of a bacterial MoeB−MoaD complex, *Nature 414*, 325−329.
8. Walden, H., Podgorski, M. S., Huang, D. T., Miller, D. W., Howard, R. J., Minor, D. L., Jr., Holton, J. M., and Schulman, B. A. (2003) The structure of the APPBP1-UBA3-NEDD8-ATP complex reveals the basis for selective ubiquitin-like protein activation by an E1, *Mol. Cell 12*, 1427−1437.
9. Schwartz, D. C., and Hochstrasser, M. (2003) A superfamily of protein tags: ubiquitin, SUMO and related modifiers, *Trends Biochem. Sci. 28*, 321−328.
10. Otwinowski, Z., and Minor, W. (1997) Processing of X-ray diffraction data collected in oscillation mode, *Methods Enzymol. 276*, 307−326.
11. Terwilliger, T. C., and Berendzen, J. (1999) Automated structure solution for MIR and MAD (http://www.solve.lanl.gov), *Acta Crystallogr. D55*, 849−861.
12. Brünger, A. T., Adams, P. D., Clore, G. M., DeLano, W. L., Gros, P., Grosse-Kunstleve, R. W., Jiang, J. S., Kuszewski, J., Nilges, M., Pannu, N. S., Read, R. J., Rice, L. M., Simonson, T., and Warren, G. L. (1998) Crystallography & NMR system: A new software suite for macromolecular structure determination, *Acta Crystallogr. D54*, 905−921.
13. Jones, T. A., Zou, J.-Y., Cowan, S. W., and Kjeldgaard, M. (1991) Improved methods for the building of protein models in electron density maps and the location of errors in these models., *Acta Crystallogr. A47*, 110−119.
14. Kleygert, G. J., and Jones, T. A. (1996) xdlMAPMAN and xdlDATAMAN-programs for reformatting, analysis, and manipulation of biomacromolecular electron-density maps and reflection datasets, *Acta Crystallogr. D52*, 826−828.
15. Murshudov, G. N., Vagin, A. A., Lebedev, A., Wilson, K. S., and Dodson, E. J. (1999) Efficient anisotropic refinement of macromolecular structures using FFT, *Acta Crystallogr. D55* (Part 1), 247−255.
16. Beu, S. C., Senko, M. W., Quinn, J. P., Wampler, F. M., III, and McLafferty, F. W. (1993) Fourier transform electrospray instrumentation for tandem high-resolution mass spectrometry of large molecules, *J. Am. Soc. Mass Spectrom. 4*, 557−565.
17. van Aalten, D. M., Bywater, R., Findlay, J. B., Hendlich, M., Hooft, R. W., and Vriend, G. (1996) PRODRG, a program for generating molecular topologies and unique molecular descriptors from coordinates of small molecules, *J. Comput.-Aided Mol. Des. 10*, 255−262.
18. Vijay-Kumar, S., Bugg, C. E., Wilkinson, K. D., Vierstra, R. D., Hatfield, P. M., and Cook, W. J. (1987) Comparison of the three-dimensional structures of human, yeast, and oat ubiquitin, *J. Biol. Chem. 262*, 6396−6399.

19. Rudolph, M. J., Wuebbens, M. M., Rajagopalan, K. V., and Schindelin, H. (2001) Crystal structure of molybdopterin synthase and its evolutionary relationship to ubiquitin activation, *Nat. Struct. Biol. 8*, 42−46.
20. Dorrestein, P. C., Zhai, H., McLafferty, F. W., and Begley, T. P. The Sulfur Transfer Mediated by the Sulfur Carrier Protein ThiS, *Chem. Biol.*, submitted for publication.
21. Holm, L., and Sander, C. (1993) Protein structure comparison by alignment of distance matrices, *J. Mol. Biol. 233*, 123−138.
22. Lorentzen, E., Pohl, E., Zwart, P., Stark, A., Russell, R. B., Knura, T., Hensel, R., and Siebers, B. (2003) Crystal structure of an archaeal class I aldolase and the evolution of (βα)8 barrel proteins, *J. Biol. Chem. 278*, 47253−47260.
23. Lorentzen, E., Siebers, B., Hensel, R., and Pohl, E. (2004) Structure, function and evolution of the Archaeal class I fructose-1,6-bisphosphate aldolase, *Biochem. Soc. Trans. 32*, 259−263.
24. Jia, J., Schorken, U., Lindqvist, Y., Sprenger, G. A., and Schneider, G. (1997) Crystal structure of the reduced Schiff-base intermediate complex of transaldolase B from *Escherichia coli*: mechanistic implications for class I aldolases, *Protein Sci. 6*, 119−124.
25. Whitby, F. G., Xia, G., Pickart, C. M., and Hill, C. P. (1998) Crystal structure of the human ubiquitin-like protein NEDD8 and interactions with ubiquitin pathway enzymes, *J. Biol. Chem. 273*, 34983−34991.
26. Bohnsack, R. N., and Haas, A. L. (2003) Conservation in the mechanism of Nedd8 activation by the human AppBp1-Uba3 heterodimer, *J. Biol. Chem. 278*, 26823−26830.
27. Chiu, H. J., Reddick, J. J., Begley, T. P., and Ealick, S. E. (1999) Crystal structure of thiamin phosphate synthase from *Bacillus subtilis* at 1.25 Å resolution, *Biochemistry 38*, 6460−6470.
28. Choi, K. H., Mazurkie, A. S., Morris, A. J., Utheza, D., Tolan, D. R., and Allen, K. N. (1999) Structure of a fructose-1,6-bis(phosphate) aldolase liganded to its natural substrate in a cleavage-defective mutant at 2.3 Å, *Biochemistry 38*, 12655−12664.
29. Kraulis, P. J. (1991) MOLSCRIPT: a program to produce both detailed and schematic plots of protein structures, *J. Appl. Crystallogr. 24*, 946−950.
30. Merritt, E. A., and Bacon, D. J. (1997) Raster3D: Photorealistic Molecular Graphics, *Methods Enzymol. 277*, 505−524.
31. Christopher, J. A. (1998) Spock computer program, Texas A&M University, College Station, TX.

BI0488911